Lyapunov spectrum of granular gases

Sean McNamara and Michel Mareschal
Centre Européen de Calcul Atomique et Moléculaire, Ecole Normale Supérieure de Lyon, 46 allée d'Italie, 69364 Lyon Cedex 07, France

(Received 5 December 2000; published 22 May 2001)

We calculate and study the Lyapunov spectrum of a granular gas maintained in a steady state by an isokinetic thermostat. Considering restitution coefficients greater than unity allows us to show that the spectra change smoothly and continuously at equilibrium. The shearing instability of the granular gas, however, provokes an abrupt change in the structure of the spectrum. The relationship between various physically relevant quantities and the energy dissipation rate differs from previously studied nonequilibrium steady states.

DOI: 10.1103/PhysRevE.63.061306 PACS number(s): 45.70.−n, 05.45.Jn, 05.70.Ln

I. INTRODUCTION

The Lyapunov spectra of several nonequilibrium systems have recently been studied and calculated [1–8]. These nonequilibrium steady states are generated by traditional nonequilibrium molecular dynamics (NEMD) simulations, and are constructed by forcing a system while adding a thermostat to remove the dissipated energy. The most common example is a shear imposed onto a fluid, with a Gaussian or Nosé-Hoover thermostat [9] added to remove the energy dissipated by the viscosity. In these systems, the sum of all the Lyapunov exponents is proportional to the energy dissipation rate and can thus be linked to the transport coefficients. Furthermore, the spectra of many of these systems often have a special symmetry that simplifies the calculation of their sum. An alternative method of calculating transport coefficients from Lyapunov spectra has been proposed [10,11]. For a review, see Ref. [12].

In this paper, we study the Lyapunov spectrum of granular gases. Granular gases [13–17] are a generalization of an early model of fluids, the hard-sphere fluid [18]. The Lyapunov spectrum of the hard-sphere fluid has already been studied [6,19,20], giving us a well defined point of comparison. The hard-sphere fluid is a set of spheres (or disks in two dimensions) that move freely through space, interacting only during instantaneous, energy-conserving collisions. In granular gases, we allow collisions to dissipate or generate energy. The change of energy depends on a single parameter r, the restitution coefficient. When $r=1$, collisions conserve energy, and we recover the hard-sphere fluid. The change in energy during collisions is compensated by a Gaussian thermostat, as in the previously studied NEMD systems.

The granular gas thus resembles the NEMD systems, but there are several important differences. The most fundamental is that the granular gas has irreversible microscopic dynamics. Another important difference is that the granular gas does not have a thermodynamic limt. For any fixed value of $r\neq 1$, instabilities appear as N is increased. Furthermore, for the granular gas, equilibrium can be approached continuously from two directions: $r\to 1_-$ and $r\to 1_+$. In the NEMD systems, equilibrium can be approached from only one direction, by letting the forcing tend to 0.

We will compare the Lyapunov spectra of granular gases with those of NEMD systems. For both these systems, the Lyapunov exponents and their derivatives are continuous at equilibrium, and the sum of the exponents and the dimension of the attractor are extensive quantities. Unlike NEMD systems, however, the sum of granular gas spectra is not linear in the energy dissipation rate, but quadratic. The sums of certain pairs of exponents, however, are proportional to the dissipation rate. When r is lowered below a certain threshold, the granular gas becomes unstable. This instability has a dramatic effect on the Lyapunov spectrum.

A. Lyapunov spectrum

The Lyapunov exponents describe how quickly two identical systems with almost identical initial conditions diverge in phase space. Consider a system at the point $\mathbf{\Gamma}(0)$ in phase space of L dimensions. The system follows some trajectory through phase space, arriving at $\mathbf{\Gamma}(t)$ at time t. We express this mathematically by defining $\mathcal{S}_t$ to be an operator that evolves a point in phase space forward a time t,

$$\mathbf{\Gamma}(t)=\mathcal{S}_t\mathbf{\Gamma}(0). \tag{1}$$

Next, consider a second system at at $\mathbf{\Gamma}+\delta\mathbf{\Gamma}$, where $\delta\mathbf{\Gamma}$ is infinitesimally small. After a time t, this system moves to

$$\mathbf{\Gamma}(t)+\delta\mathbf{\Gamma}(t)=\mathcal{S}_t[\mathbf{\Gamma}(0)+\delta\mathbf{\Gamma}(0)]. \tag{2}$$

Then the Lyapunov exponent λ is defined to be

$$\lambda=\lim_{t\to\infty}\frac{1}{t}\ln\frac{|\delta\mathbf{\Gamma}(t)|}{|\delta\mathbf{\Gamma}(0)|}. \tag{3}$$

Note that λ has units of inverse time. It is thus the growth (or decay) rate of the perturbation $\delta\mathbf{\Gamma}$. In general λ is a function of both $\mathbf{\Gamma}$ and $\delta\mathbf{\Gamma}$. This is unfortunate, because both $\mathbf{\Gamma}$ and $\delta\mathbf{\Gamma}$ contain L numbers, so that λ is a function on a $2L$ dimensional space. However, the situation can be improved because the $\delta\mathbf{\Gamma}$ are infinitesimal. This means that their evolution depends only on the linearized dynamics,

$$\mathbf{\Gamma}(t)+\delta\mathbf{\Gamma}(t)=\mathcal{S}_t\mathbf{\Gamma}(0)+\mathcal{M}\cdot\delta\mathbf{\Gamma}, \tag{4}$$

where $\mathcal{M}$ is simply an $L\times L$ matrix. Since $\mathcal{M}$ is a linear operator, knowing $\lambda(\mathbf{\Gamma},\delta\mathbf{\Gamma})$ for a set of $\delta\mathbf{\Gamma}$ that spans the phase space enables one to calculate $\lambda(\mathbf{\Gamma},\delta\mathbf{\Gamma})$ for any $\delta\mathbf{\Gamma}$.

By convention, we associate λ_1 with the fastest growing direction $\delta\mathbf{\Gamma}_1$; λ_2 with the fastest growing direction $\delta\mathbf{\Gamma}_2$ that is also perpendicular to $\delta\mathbf{\Gamma}_1$ ($\delta\mathbf{\Gamma}_1 \cdot \delta\mathbf{\Gamma}_2 = 0$), and λ_i with the fastest growing direction $\delta\mathbf{\Gamma}_i$ with $\delta\mathbf{\Gamma}_j \cdot \delta\mathbf{\Gamma}_i = 0$ for $j < i$.

Furthermore, for ergodic systems, the Lyapunov spectrum $\{\lambda_i\}$ is independent of $\mathbf{\Gamma}$. This enables us to do away with the dependence on $\mathbf{\Gamma}$, and speak about *the* Lyapunov spectrum of a system. A dynamical system is ergodic if its invariant distribution cannot be subdivided into smaller invariant pieces. This is a more general condition than equilibrium: systems out of equilibrium can also be ergodic. In this paper, we will assume that all the systems considered here are ergodic, although this has not been proved. However, we have not seen anything that would contradict this assumption.

B. Granular materials

By a granular material, we mean substances such as sand, powders, grain, or gravel that are composed of many individual macroscopic particles. We consider an idealization of these materials called the inelastic hard sphere model. This model is a generalization of the hard-sphere fluid, an early model of liquids [18]. In the hard-sphere fluid, particles are assumed to move freely, without interaction, except during instantaneous collisions, when the particle velocities change discontinuously. Forces between the particles are never calculated; instead the post collisional velocities are calculated directly from the precollisional velocities and positions using a ''collision rule.'' The collision rule is derived by assuming that a collision conserves momentum and energy, and that the force between the particles acts only along a line connecting the centers of the particles. When modeling granular materials, we wish to remove energy conservation, because collisions between macroscopic particles do not conserve the macroscopic kinetic energy. Thus, we replace the conservation of energy by the definition of the restitution coefficient r. If $\hat{n}$ is a unit vector pointing along the line of centers, and the primed (unprimed) velocities are the post-collisional (precollisional) velocities, then

$$(\vec{v}_A' - \vec{v}_B') \cdot \hat{n} = -r(\vec{v}_A - \vec{v}_B) \cdot \hat{n}, \tag{5}$$

where the subscripts A and B denote the colliding particles. Throughout this paper we use boldface letters to indicate vectors in phase space, and mark physical space vectors with an arrow or a hat. Equation (5) says that the relative velocity along the line of centers is reversed and reduced by a factor of r. The four assumptions can be combined to give the collision rule,

$$\vec{v}_A' = \vec{v}_A + \vec{f}, \quad \vec{v}_B' = \vec{v}_B - \vec{f}, \tag{6}$$

$$\text{where } \vec{f} \equiv \frac{1+r}{2}[(\vec{v}_B - \vec{v}_A) \cdot \hat{n}]\hat{n}.$$

The change in energy during a collision is

$$\Delta E = -\frac{1}{4}(1-r^2)[(\vec{v}_B - \vec{v}_A) \cdot \hat{n}]^2. \tag{7}$$

If $r = 1$, energy is conserved during collisions, and we have the traditional hard-sphere fluid. One usually considers only $r < 1$, because collisions always dissipate energy in experimental granular flows. We will also consider the case $r > 1$ (collisions generate energy), which is unphysical, but provides access to two different equilibrium limits: $r \to 1_+$ and $r \to 1_-$.

C. The freely cooling granular gas

In this paper, we consider exclusively the two-dimensional freely cooling granular gas. To perform this simple computer experiment, N identical disks of radius a are placed in a periodic domain of size L_x by L_y. The initial conditions are drawn from the microcanonical ensemble: the total energy is fixed, the disks are uniformly distributed in space and given velocities drawn from the Maxwell-Boltzmann distribution. The system then evolves without any input of energy. This experiment was invented by Haff [13], and is now the subject of many papers [14–17].

At $r = 1$, we recover the hard-sphere fluid in equilibrium: the density remains homogeneous and the velocities obey the Maxwell-Boltzmann distribution. As r decreases, nothing dramatic seems to happen: the density remains constant, and no large scale motion is visible (although there are subtle differences with the equilibrium state). This situation is called the ''homogeneous cooling state'' because the granular temperature (the average kinetic energy per particle) remains spatially uniform but decreases monotonically with time. As r decreases, the temperature decreases more and more rapidly. Finally, r reaches some critical value, where a transition to a shearing state appears: the particles spontaneously form two countermoving streams. This instability occurs when the randomized kinetic energy of the granular temperature decays more rapidly than the longest shear modes. This process has been studied in detail using a hydrodynamic approach [17], and it has a dramatic effect on the Lyapunov spectrum. As r decreases further, the dense clusters form. When $r > 1$, the density remains constant. When r becomes much larger than 1, all the kinetic energy becomes concentrated in a few particles.

But there is a problem: the freely cooling granular medium is not in a steady state. The total energy is monotonically decreasing (or increasing for $r > 1$). However, a long time average over a steady state is needed to calculate the Lyapunov exponents. A steady state can be created by multiplying the velocities of all the particles by

$$\epsilon = \sqrt{\frac{E_0}{E_0 + \Delta E}} \tag{8}$$

just after each collision. Here, E_0 is the (constant) total kinetic energy and ΔE, given in Eq. (7), is the change in energy during a collision. The advantage of this method is that multiplying all the velocities by a constant does not change the sequence of collisions, it only makes them occur sooner (or later). This means that it is not necessary to multiply all the velocities at each collision. One simply replaces the usual time variable t with a new time variable s,

$$s \equiv \int \gamma \, dt, \quad \gamma \equiv \sqrt{\frac{E^{(t)}(t)}{E_0}}. \tag{9}$$

Here, $E^{(t)}(t)$ is the total kinetic energy, measured in terms of the original, unadjusted time t, and E_0 is the kinetic energy at $t=0$. Changing the time variable from t to s necessitates transforming the velocities because they are simply derivatives of position with respect to time,

$$v^{(s)} = v^{(t)}/\gamma. \tag{10}$$

Note that a particle in free motion ($v^{(t)}$ constant) will seem to accelerate or deaccelerate as γ changes with time. In terms of the transformed velocities, the total kinetic energy is constant: $E^{(s)} = E^{(t)}/\gamma^2 = E_0$.

D. The Lyapunov spectra of NEMD systems

The thermostat used to keep the granular gas in a steady state is a discrete time version of the Gaussian or isokinetic thermostat, where the total energy is maintained constant by applying a small drag to all the particles. This thermostat has often been used in NEMD studies. For continuous time, applying this thermostat gives equations of motion with the form,

$$\dot{\mathbf{\Gamma}} = \begin{pmatrix} \dot{\boldsymbol{r}} \\ \dot{\boldsymbol{v}} \end{pmatrix} = \boldsymbol{F}(\mathbf{\Gamma}) - \alpha \begin{pmatrix} \mathbf{0} \\ \boldsymbol{v} \end{pmatrix}. \tag{11}$$

Setting $\alpha = 0$ gives the unthermostatted system. For the Gaussian thermostat, α is adjusted at every time step to keep the energy constant. This thermostat samples the microcanonical (isokinetic) ensemble. The Nosé-Hoover thermostat gives equations of motion written in the same form, except that α obeys $\dot{\alpha} = [(E_0/E) - 1]/\tau^2$ (where τ is the response time of the thermostat). The Nosé-Hoover thermostat allows the energy E to fluctuate about its mean E_0, and samples the canonical, or isothermal ensemble. The Nosé-Hoover thermostat reduces to the Gaussian thermostat in the limit $\tau \to 0$. For both thermostats, $\langle \alpha \rangle$ is proportional to the energy dissipation rate.

The Gaussian thermostat, the Nosé-Hoover thermostat, and the ''granular Gaussian'' thermostat presented in the previous section are all very similar. They all maintain a constant energy by rescaling the velocities. The Nosé-Hoover thermostat can also be understood as a time rescaling [9], just like the granular Gaussian thermostat in Sec. I C. However, the time-rescaling formulation of the Nosé-Hoover thermostat is difficult to implement, so the velocity-rescaling formulation is used more frequently. The velocity-rescaling formulation is also easier to understand. For granular gases, the situation is different. As discussed in the previous section, the time-rescaling formulation is computationally more efficient; therefore the time-rescaling formulation is used in the simulations presented in this paper. However, we will discuss the results from the velocity-rescaling perspective, because this makes them easier to understand.

The Lyapunov spectra of several thermostatted systems have been calculated [1–8]. We will compare the spectra of these systems to those of granular gases, emphasizing two points: (1) the relation between sums of the exponents and the energy dissipation rate, and (2) the validity of the conjugate pairing rule.

The proportionality of the sum of the exponents to the energy dissipation rate has been used to express the transport coefficients in terms of Lyapunov spectra. For example, in uniform shear, the energy dissipation rate is $\eta\gamma^2$ where γ is the shear rate and η is the dynamic viscosity. One can therefore write $\eta \sim (\Sigma\lambda)/\gamma^2$.

The validity of the conjugate pairing rule greatly simplifies the calculation of $\Sigma\lambda$ [2,5]. This rule states that conjugate pairs of exponents sum to $-\langle \alpha \rangle$. The smallest and the largest exponent form one conjugate pair, the second smallest and the second largest another pair, etc. In our two-dimensional system with $4N$ degrees of freedom, the conjugate pairing rule states,

$$\lambda_i + \lambda_{4N-i+1} = -\langle \alpha \rangle, \quad \text{for } 1 \leqslant i \leqslant 4N. \tag{12}$$

If the conjugate pairing rule holds, $\Sigma\lambda$ can be calculated from any pair of exponents. In Sec. II B, we show that certain conjugate pairs of granular gases obey Eq. (12), but the majority do not.

E. Computational details

1. Units

All results in this paper are numerical, and given in nondimensional units. We use the particle radius a as the unit of distance, and the particle mass m defines the unit of mass. The unit of time is defined by fixing $\Sigma v_i^2 = N$, where v_i is the velocity of particle i. (Thus the total energy is $E_0 = N/2$.) All numerical data shown in the figures is given in terms of these units. For example, the notation $L_y = 45$ in various figure captions means that the simulational domain has a height of 45 particle radii.

2. Algorithm

Since the inelastic hard sphere model is a generalization of the hard-sphere fluid, we modify Dellago and Posch's algorithm [6] for calculating the Lyapunov spectrum of a hard-sphere fluid. In the Appendix, we discuss certain subtleties that arise because we calculate the Lyapunov spectrum in terms of s and not t.

II. STRUCTURE OF THE SPECTRUM

We will first discuss the structure of the Lyapunov spectrum at $r=1$ (equilibrium), and then show how this structure changes with r. Much of what we present in Sec. II A has already been discussed in Ref. [20], but this material is needed for the interpretation of the nonequilibrium spectra in Sec. II B.

A. Equilibrium spectra

At $r=1$, conjugate pairs of exponents sum to 0: $\lambda_i + \lambda_{4N-i+1} = 0$. Thus, each exponent has a partner that is

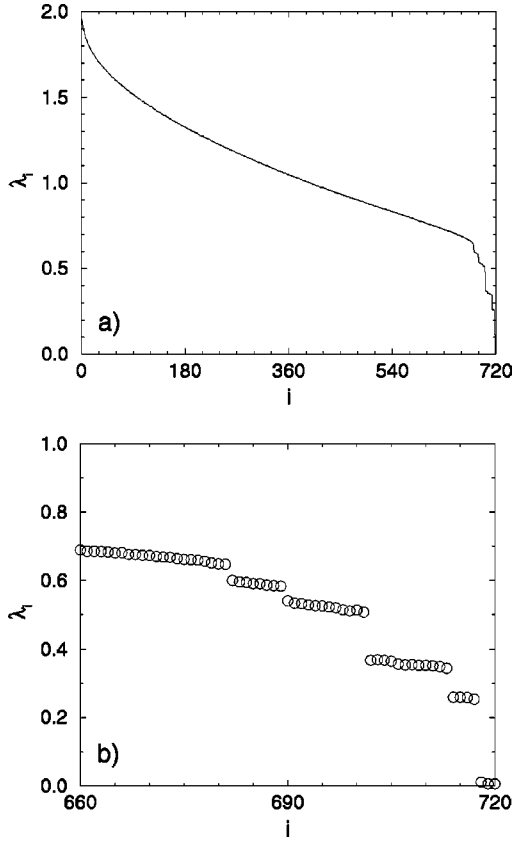

FIG. 1. The spectrum of a $N=360$ hard-disk fluid ($r=1$) in a square domain ($L_x=L_y=45$). (a) The first $2N$ Lyapunov exponents (the second $2N$ are just the negative of the exponents shown). (b) The smallest positive exponents (note difference in the x axis). For an explanation of the units used in this figure, see Sec. I E 1.

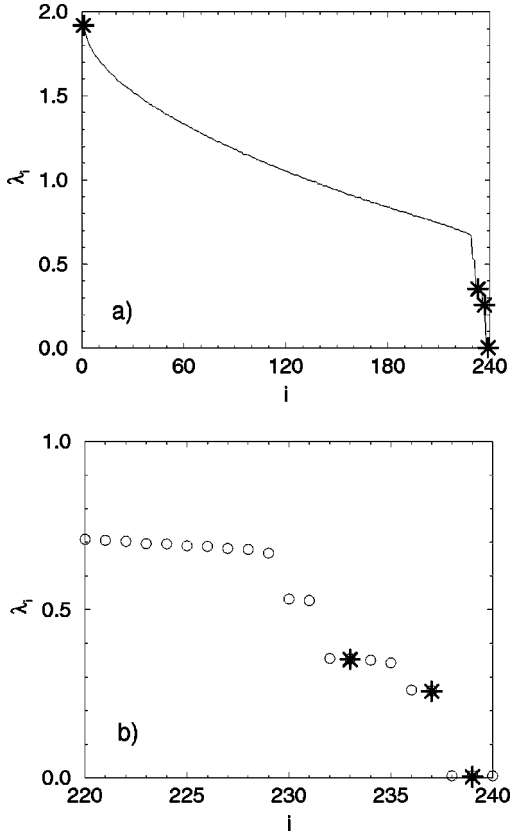

FIG. 2. The same as Fig. 1, but for a $N=120$ hard-disk fluid in a rectangular domain. ($r=1$, $L_x=15$, $L_y=45$.) The density is the same as in Fig. 1, but L_x is reduced by one third. The stars mark the exponents featured in Fig. 3.

exactly its negative, and it is necessary to calculate only half the spectrum. The second half contains no additional information, and is simply the negative of the first.

In Fig. 1, we show half of a typical spectrum of the hard-sphere fluid at equilibrium. The parameters of the system are $N=360$, $L_x=L_y=45$. The spectrum can be divided into two parts. For $i\leqslant 681$, the exponents fall onto a well defined continuous curve. On the other hand, for $682\leqslant i\leqslant 720$, the exponents appear in small groups at discrete values.

The discrete groups of exponents have been discussed by Posch and Hirschl [20]. They correspond to hydrodynamic-like perturbations, and appear in groups of four and eight in Fig. 1 because there are fourfold or eightfold degeneracies associated with the square domain. If we break the symmetry of the simulational domain by setting $L_x\neq L_y$, the groups of exponents separate into two parts. When either L_x or L_y is small, several groups of exponents disappear, and the discrete part of the spectrum is simplified. Therefore, it is useful to consider a narrow ($L_x=L_y/3$) system with the same density. This system is shown in Fig. 2.

We now want to investigate the physical processes underlying the exponents. As discussed in Sec. I A, each exponent λ_i gives the growth rate of a perturbation in phase space $\delta\mathbf{\Gamma}_i$. Each $\delta\mathbf{\Gamma}_i$ has $4N$ components: $2N$ give the displacements of each particle in physical space, and the other $2N$ give their displacements in momentum space. We denote the displacement in physical space of particle j as $\delta\vec{r}_j^{\,(i)}$ and its velocity space displacement as $\delta\vec{v}_j^{\,(i)}$. It is helpful to visualize the Lyapunov vectors $\delta\mathbf{\Gamma}_i$ by projecting the $\delta\vec{r}_j$ or $\delta\vec{v}_j$ onto the positions of the corresponding particles. This is done in Fig. 3, where we show five typical vectors, one from the continuous part of the spectrum, and the rest from the discrete part.

The continuous part of the spectrum [represented by $\delta\mathbf{\Gamma}_1$ in Fig. 3(a)] corresponds to disorganized and local perturbations. Many particles have very small contributions to $\delta\mathbf{\Gamma}_1$. As the Lyapunov index i increases, the modes become less local: more and more particles have significant amplitudes, but the modes remain disorganized. These modes are also very time dependent. If the simulation were to run a bit longer or a bit shorter, the set of contributing particles would change, and Fig. 3(a) would look completely different. On the other hand, if the calculations were started with a different initial $\delta\mathbf{\Gamma}_1$ (but the same initial particle velocities and positions, i.e. the same initial $\mathbf{\Gamma}$) and run for the same length of time, Fig. 3(a) would not change at all.

In the discrete part of the spectrum, the exponents correspond to collective motions of the particles. This explains why these exponents appear in small separated groups at discrete values. For example, $\lambda_{236}=\lambda_{237}$ because both exponents correspond to transverse, sinusoidal shearing perturba-

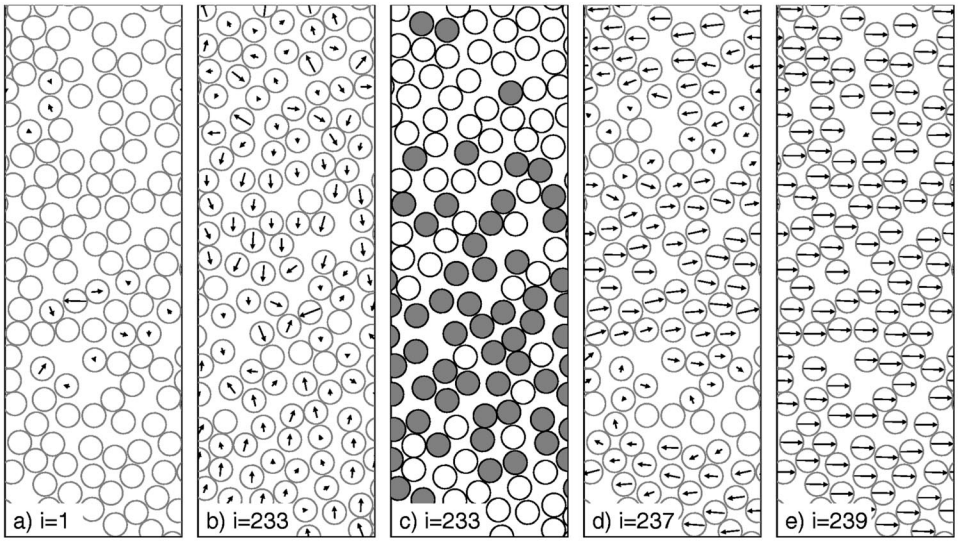

FIG. 3. Lyapunov vectors $\delta\mathbf{\Gamma}_1$, $\delta\mathbf{\Gamma}_{233}$, $\delta\mathbf{\Gamma}_{237}$, and $\delta\mathbf{\Gamma}_{239}$ of a hard-disk fluid with $N=120$, $r=1$, $L_x=15$, and $L_y=45$. The circles show the positions of the particles at the end of the simulation. In panels a, b, d, and e, the arrows show $\delta\vec{r}_j^{(i)}$, the components of $\delta\mathbf{\Gamma}_i$ that describe the displacement in physical space of particle j. (The displacements in velocity space $\delta\vec{v}_j^{(i)}$ are nearly equivalent.) The lengths of the vectors are scaled by the maximum length. If the length of a vector is less than 0.16, no vector is shown. In panel c, we shade the particles with $\delta\vec{r}_j\cdot\vec{v}_j>0$.

tions [$\delta\mathbf{\Gamma}_{237}$ is shown in Fig. 3(d), and $\delta\mathbf{\Gamma}_{236}$ is the same, but with a phase shift of $\pi/2$]. Higher harmonics of the shear waves also exist. The pair of exponents λ_{231} and λ_{230} corresponds to transverse shear waves with a wavelength of $L_y/2$. Note also that $\lambda_{230}=\lambda_{231}\approx 2\lambda_{237}$. As L_y is increased further, it is possible to see the third harmonic, then the fourth, and so on.

The exponents λ_{232} through λ_{235} corresponds to longitudinal waves, where compressive motion is coupled to a heating or cooling of the gas. (In Fig. 3, we show position perturbations $\delta\vec{r}_j$ not velocity perturbations $\delta\vec{v}_j$, but for nonzero vectors, these two quantities are closely correlated.) These waves resemble sound waves, but they do not have the same relation between velocity and position displacements. In true sound waves, the velocity and position displacements are out of phase, but in the longitudinal Lyapunov waves, the two displacements have the same phase. Furthermore, these waves do not propagate at the sound speed, but they do have higher harmonics just as the shear waves.

In general, the Lyapunov exponents in the discrete part of the spectrum obey

$$\lambda\sim\frac{n}{L_y}+O(1/L_y^2),\quad n=0,1,\ \ldots, \tag{13}$$

where n is the mode number. (The zero modes can be considered the $n=0$ members of this series.) The existence of longitudinal and transverse modes and the dependence of their exponents on their wavelengths has already been discussed [20]. Equation (13) also appears in a mathematical model of the Lyapunov exponents [21]. In another paper [22], we study these hydrodynamic modes in more detail. In the following, we refer to the transverse modes as ''sound'' modes and the longitudinal modes as ''sound'' modes, but their connection (if any) to the actual shear and sound waves of the hard-sphere fluid is an open question.

B. Nonequilibrium Lyapunov spectra

We now take the rectangular system of Fig. 2 and Fig. 3 and vary r. The results are shown in Fig. 4. We emphasize that the exponents change smoothly and continuously at equilibrium ($r=1$, the thin vertical line). If we follow a

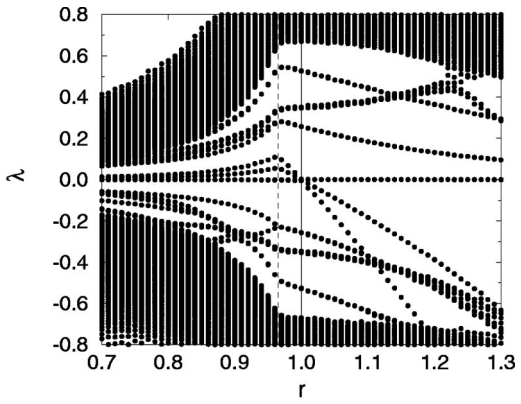

FIG. 4. The Lyapunov spectra of the freely cooling granular gas with $N=120$, $L_x=15$, $L_y=45$, and $0.7\leqslant r<1.3$. Equilibrium ($r=1$) is marked with a thin solid line, and the transition to the shearing state at $r\approx 0.965$ is marked with the dashed line. The spectrum shown in Fig. 2 appears as a single column at $r=1$; for each exponent, a dot is placed on the graph. Since all the exponents of Fig. 2 have the same value of r, they fall in a vertical column. The spectra for the other values of r are displayed in the same way. This method of graphing allows the eye to easily follow the evolution of λ with r. These spectra were computed by averaging over 2000 collisions per particle.

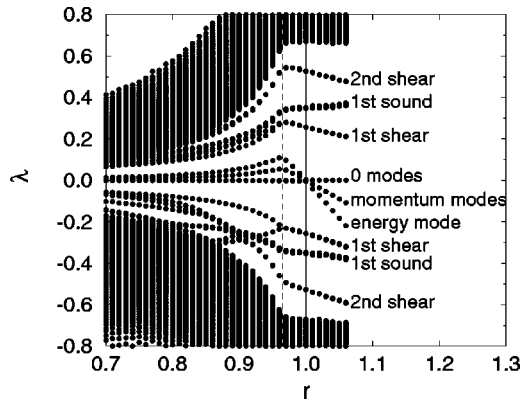

FIG. 5. A subset of the data of Fig. 4, with the different discrete exponents labeled. ''2nd shear'' is the second harmonic of the shear mode, ''1st sound'' is the first harmonic of the sound mode, [Fig. 3(b,c)], and ''1st shear'' is the first harmonic of the shear mode [Fig. 3(d)]. These three families have both a positive and a negative branch. ''0 modes'' are the three modes that remain zero for all values of r (see text). The ''momentum modes'' are modes where the momentum of each particle is increased by constant. The ''energy mode'' is where the energy of each particle is augmented by a constant.

single exponent as a function of r, nothing distinguishes the equilibrium state. On the other hand, the shearing instability (vertical dashed line) provokes abrupt changes in all the exponents. On the level of the microscopic dynamics, the shearing transition is more significant than equilibrium.

To discuss the variation of the discrete part of the spectrum with r, we present a subset of the data in Fig. 5, identifying the different families of exponents on the graph. Consulting this figure, we can see how the exponent associated with each type of hydrodynamic disturbance changes with r. The two series of points labeled ''2nd shear'' are the second harmonic of the shear mode. For $r>0.965$, both the negative and positive branches decrease as r increases. The first harmonic of the shear mode ''1st shear'' has the same behavior. At the shearing instability ($r=0.965$), the negative branch of the first shearing mode bifurcates. The degeneracy between the two shear modes is broken by the presence of shear in the system. One of the modes corresponds to a shear perturbation that is in phase with the shear in the velocities, the other is out of phase. The sound waves ''1st sound'' have a different behavior: the positive branch increases with r while the negative branch decreases.

The series of points labeled ''0 modes'' are the three modes that remain zero for all values of r. Two of these modes correspond to a uniform displacement of all the particles in physical space [as shown in Fig. 3(e)]. The third corresponds to the vector that points along the trajectory in phase space: the physical space displacements in $\delta\mathbf{\Gamma}$ are parallel to the velocities in $\mathbf{\Gamma}$.

The momentum modes are modes where all the particles are displaced uniformly in velocity space. These modes are zero at equilibrium, but become nonzero due to the effect described in Eq. (10): if the center of mass has a small initial velocity, the thermostat will amplify or diminish this movement as it adds or removes energy. The energy mode corresponds to a phase space displacement that augments the energy of each particle. This perturbation grows at twice the rate of the momentum modes.

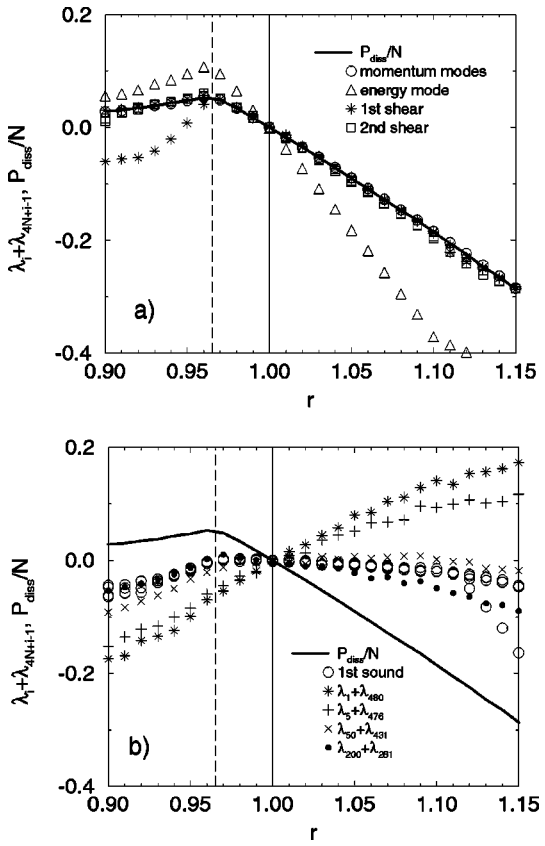

FIG. 6. Conjugate pairs of selected exponents, compared to the energy dissipation rate per particle, $P_{\rm diss}/N$. The exponents labeled in Fig. 5 are given the same names here. Four additional pairs of exponents (1,480), (5,476), (50,431), and (200,283) are shown in (b).

Another way to examine the dependence of the Lyapunov spectrum on r is to calculate conjugate pairs. In Fig. 6, we show the sums of several pairs, as well as the energy dissipation rate per particle. If the granular gas behaved as a thermostatted NEMD system, all the conjugate pairs would fall on the heavy line. It is interesting to note that the momentum and shearing modes do indeed behave in this way. Other pairs, however, do not. For example, the conjugate pair (1,480) has a slope of the opposite sign, and other pairs are nearly independent of r.

Another fact that emerges from Fig. 6 is that the conjugate sum of the shearing modes is independent of their wavelength. This is also true of the sound modes; if their second harmonic were present, its conjugate sums would fall on top of the points labeled ''1st sound'' in Fig. 6(b).

In Fig. 7, we show the Lyapunov spectrum of the square system with the same parameters as Fig. 1 ($N=360$, $L_x=L_y=45$). For $r>0.965$, the evolution of the spectra are similar to the narrow rectangular case. The shearing and sound modes have the same dependence on r. Near the second harmonic of the shearing mode, many new modes appear that were not present in the narrow rectangular system.

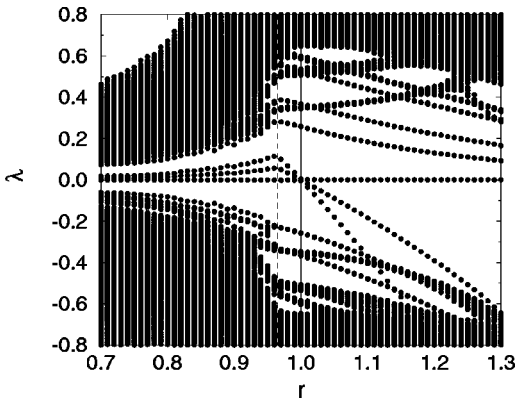

FIG. 7. Same as Fig. 4, except for a square system with three times as many particles ($N=360$, $L_x=L_y=45$).

One can easily see if they are shearing or compressive by examining their dependence on r. On the other hand, when $r<0.965$, there is a difference between the square and rectangular cases. In the rectangular case, the hydrodynamic modes maintain their identity for $r<0.965$. In the square case, the hydrodynamic modes become smeared together for $r<0.965$. This probably occurs because shearing motion disrupts any hydrodynamic mode whose wave vector is not parallel to the velocity gradient. In the rectangular case, all wave vectors must point in the y direction, along the velocity gradient. In the square case, they can point in the x or y direction, or a combination of the two.

III. GLOBAL SUMS OF THE EXPONENTS

In addition to the structure of the spectrum, there are certain sums of the exponents that have physical significance. We will present these sums as functions of r, for both the narrow and square systems shown above. In all cases, it will be seen that the sums vary continuously at $r=1$, and the most abrupt change in behavior always occurs at the onset of the shearing instability, not at equilibrium.

First of all, the sum of all the exponents give the rate of phase space contraction. In Fig. 8, we show the dependence of the sum of the whole spectrum on r. As expected, the sum is 0 at $r=1$ and negative elsewhere. The sum approaches its maximum smoothly and continuously, (although the second derivative may change abruptly at $r=1$).

The vanishing derivative of $\Sigma\lambda$ with respect to r at $r=1$ implies that there are relations between the different conjugate pairs of exponents. The sum of all the pairs must be $\Sigma\lambda$, so if certain pairs of exponents have a nonzero slope at $r=1$, as the shear modes do, there must exist other pairs whose slope has the opposite sign. In Fig. 6, we see that the pair (1,480) has a slope approximately one-half as large and of opposite to the shear modes. Thus, it cancels about one half of the shear modes. Since there are six shear modes present, plus the energy mode (which has a slope twice as large as the shear modes), there must be at least 16 pairs whose slopes are similar to (1,480). In fact, there are more, because the pairs at the lower edge of the continuous part of the spectrum [represented by (200,283) in Fig. 6] have very small slopes that have the same sign as the shear modes.

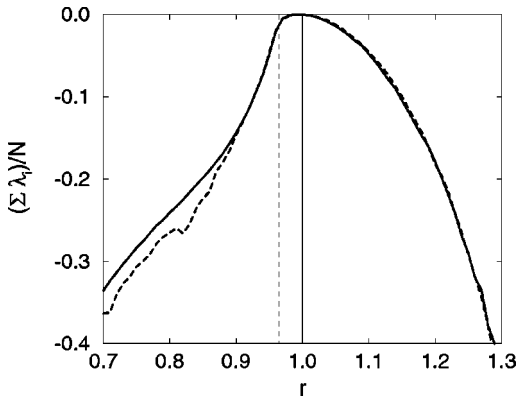

FIG. 8. The sum of the whole spectrum, divided by N. The heavy solid line is the narrow ($N=120$) system and the heavy dashed line is the square ($N=360$) system. The vertical solid line indicates equilibrium ($r=1$) and the vertical dashed line the onset of the shearing instability.

The behavior of $\Sigma\lambda$ differs from the NEMD systems, because $\Sigma\lambda$ is quadratic in the energy dissipation rate $P_{\rm diss}$. Figure 6 shows $P_{\rm diss}$, and it is linear in r. In Fig. 8, $\Sigma\lambda$ is quadratic in r and therefore also in $P_{\rm diss}$.

The Kolmogorov-Sinai entropy h_{KS} gives the rate at which a forecast made from finite precision data loses accuracy. For closed systems, like the one considered in this paper, it is equal to the sum of all the positive Lyapunov exponents. In Ref. [6], this quantity has been calculated as a function of density and shown to be closely related to the collision frequency. In Fig. 9, we show the Kolmogorov-Sinai entropy per particle as a function of r and as a function of collision frequency. As a function of r, h_{KS} is continuous at equilibrium, and seems to have a maximum at a value of r slightly larger than 1. The biggest change in behavior occurs at the shearing instability, where h_{KS} falls rapidly. Figure 9(b) reveals that h_{KS} is roughly proportional to the collision rate dC/ds, so that the rapid fall of h_{KS} at the onset of the shearing instability is due to the reduction of the collision rate.

Finally, the spectrum can be used to calculate the dimension of the attractor using the Kaplan-Yorke conjecture [1,4,23]. One starts adding the exponents together, starting with the λ_1. The sum increases until one reaches the 0 exponents. Then one starts adding the negative exponents, and the sum decreases. When the sum vanishes, one stops, and counts the number of exponents in the sum. This is D_L, the ''Lyapunov'' dimension of the attractor. Usually only a fraction of the last exponent is needed to make the sum vanish, so that the number of exponents in the sum is not necessarily an integer. This method has been shown to be exact up to six dimensions, and to give an upper bound in higher dimensions. For equilibrium systems, this procedure gives $4N$, the dimension of the phase space. Like $\Sigma\lambda$ in Fig. 8, D_L has a quadratic dependence on r for $r>0.965$, and thus a quadratic dependence on $P_{\rm diss}$. This is different from the NEMD systems, where D_L has a linear dependence on $P_{\rm diss}$ [4]. But like the NEMD systems, D_L is an extensive quantity, i.e., it is proportional to N. This can be seen from the nearly perfect superposition of the two lines in Fig. 10.

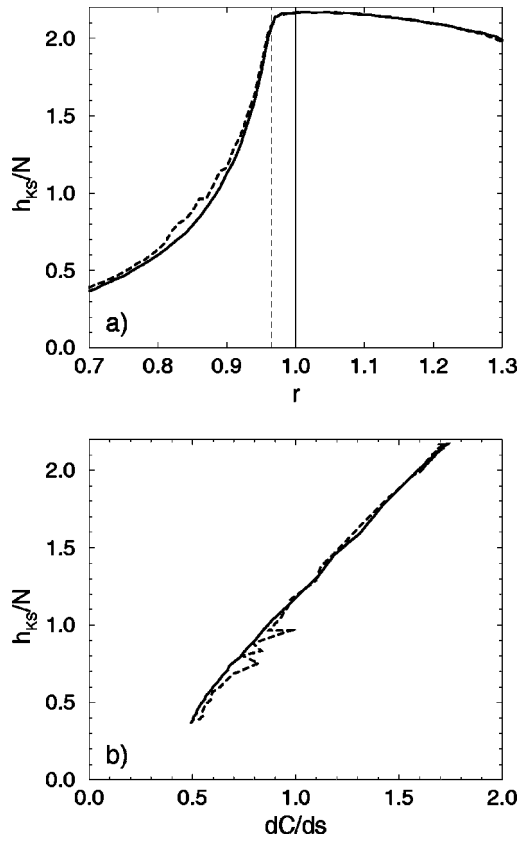

FIG. 9. The Kolomogorov-Sinai entropy divided by N. The solid line is the narrow ($N=120$) system and the dashed line is the square ($N=360$) system. (a) as a function of r, (b) as a function of collision rate dC/ds.

For $r<0.965$, D_L decreases approximately linearly with r. It may be tempting to compare this with a NEMD system, but $P_{\rm diss}$ is not linear in r for $r<0.965$, so D_L is not linear in $P_{\rm diss}$.

IV. CONSTRUCTION OF UNSTABLE TRAJECTORIES

The phase space dynamics of nonequilibrium steady states are governed by two fractal objects: the attractor and the repeller [7,24]. The attractor is the object whose dimension is shown in Fig. 10, and is the set of stable trajectories. A trajectory starting from almost any point in phase space rapidly approaches, or is ''attracted'' to, the attractor. The repellor is the set of unstable trajectories. These unstable trajectories cannot be observed directly in simulations, because any small deviation from the repellor grows exponentially. In this way, a system placed at almost any point in phase space is attracted by the attractor and repelled by the repellor.

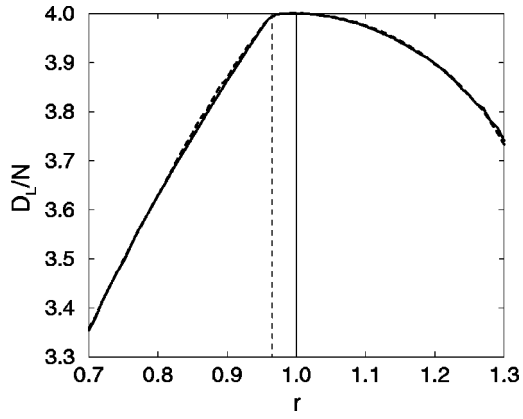

FIG. 10. The Lyapunov dimension of the attractor D_L, divided by N. The solid line is the narrow ($N=120$) system and the dashed line is the square ($N=360$) system.

In reversible systems, the repellor trajectories can be constructed by taking a simulated trajectory, and following it backwards in time. We can express this in mathematical symbols. Let $\mathbf{\Gamma}_0$ be the starting point of the simulated (attractor) trajectory and $\mathbf{\Gamma}_1$ its end. Then we have

$$\mathbf{\Gamma}_1=\mathcal{S}_t\mathbf{\Gamma}_0, \quad \mathcal{V}_-\mathbf{\Gamma}_0=\mathcal{S}_t\mathcal{V}_-\mathbf{\Gamma}_1, \tag{14}$$

where $\mathcal{V}_-$ is an operator that reverses all the velocities. The first equation expresses the attractor trajectory ($\mathbf{\Gamma}_0\to\mathbf{\Gamma}_1$) and the second the repellor trajectory ($\mathcal{V}_-\mathbf{\Gamma}_1\to\mathcal{V}_-\mathbf{\Gamma}_0$). The operator $\mathcal{S}_t$ is the same in both cases because the microscopic dynamics is reversible. Since Eq. (14) applies for any time t, the repellor is just mirror image of the attractor. We can obtain it simply by applying $\mathcal{V}_-$ to the attractor [7].

But this is not true for granular gases, because the microscopic dynamics is not reversible. But there is still a way to generate the repellor trajectories. Note that the collision rule, Eq. (6), can be rewritten as

$$\vec{v}_A=\vec{v}_A'+\vec{f}', \quad \vec{v}_B=\vec{v}_B'-\vec{f}',$$
$$\vec{f}'\equiv\frac{1+1/r}{2}[(\vec{v}_B'-\vec{v}_A')\cdot\hat{n}]\hat{n}. \tag{15}$$

This equation has the form of the collision rule, except the restitution coefficient is now $1/r$ and the pre- and post-collisional velocities have exchanged roles. A collision at restitution coefficient r is the inverse of a collision at $1/r$. Therefore, Eq. (14) must be modified to

$$\mathbf{\Gamma}_1=\mathcal{S}_t^{(r)}\mathbf{\Gamma}_0, \quad \mathcal{V}_-\mathbf{\Gamma}_0=\mathcal{S}_t^{(1/r)}\mathcal{V}_-\mathbf{\Gamma}_1, \tag{16}$$

where the superscript on $\mathcal{S}_t$ indicates the restitution coefficient. We have used this procedure to generate repellor trajectories, and computed their Lyapunov spectrum. We find a spectrum that is exactly the negative of the first. This is what is expected, because if we consider a trajectory infinitely close to the first trajectory: $\mathbf{\Gamma}_0+\delta\mathbf{\Gamma}_0\to\mathbf{\Gamma}_1+\delta\mathbf{\Gamma}_1$ that generates a Lyapunov exponent λ, we know that its image: $\mathcal{V}_-(\mathbf{\Gamma}_1+\delta\mathbf{\Gamma}_1)\to\mathcal{V}_-\mathbf{\Gamma}_0+\delta\mathbf{\Gamma}_0$ exists, and will generate the Lyapunov exponent $-\lambda$.

We emphasize that for granular gases, the repellor cannot be obtained by simply applying $\mathcal{V}_-$ to the attractor. The repellor is not the mirror image of the attractor, but the mirror image of the attractor with $r\to 1/r$.

V. CONCLUSIONS

We have calculated the Lyapunov spectrum of granular gases and explored some of its properties. In general, we find that equilibrium is distinguished only by the symmetry of the spectrum. There are no discontinuities in the spectrum at equilibrium. On the other hand, the onset of the shearing instability causes big changes in the spectrum. The onset of the shearing instability is associated with a rapid decrease in sum of the spectrum, the Kolmogorov-Sinai entropy, and the dimension of the attractor. Furthermore, the shearing instability disrupts the hydrodynamic structure of spectrum.

We compared the granular gas to the NEMD thermostatted systems whose Lyapunov spectra have been studied for several years. There are important differences between the relation of the energy dissipation rate and the sum of the Lyapunov exponents $\Sigma\lambda$. In granular gases, the sum of the Lyapunov exponents is quadratic in the energy dissipation rate, not linear as in the NEMD systems. This may be due to the existence of two different equilibrium limits: $r\to 1_+$ and $r\to 1_-$. Equilibrium $(r=1)$ must be a maximum of $\Sigma\lambda$ since $\Sigma\lambda<0$ for nonequilibrium systems. This means that the derivative of $\Sigma\lambda$ with respect to r must either vanish at $r=1$ or be discontinuous. But this second possibility is excluded because all the exponents are continuous in r.

We also showed how to construct the repellor. One cannot construct it by simply reversing the velocities of the attractor trajectories, for the microscopic dynamics is irreversible. Instead, one must reverse the velocities after changing the restitution coefficient to its reciprocal.

In conclusion, there are many points of contact between granular gases and the previously studied nonequilibrium systems. Yet, granular gases are not so similar as to be equivalent to modifying a few parameters of an existing case. It is therefore fruitful to compare granular gases with these other systems, as we have done in this paper. We hope this work will deepen the scientific community's understanding of chaos in nonequilibrium systems and suggest new directions of inquiry.

ACKNOWLEDGMENTS

We thank Stefano Ruffo, Pierre Gaspard, and Charles Dellago for several helpful discussions. We also thank Harald Posch for providing us with Ref. [20] before its publication. We thank the Centre National de la Recherche Scientifique for funding a part of this work.

APPENDIX: AN ALGORITHM FOR CALCULATING THE LYAPUNOV SPECTRUM OF A GRANULAR GAS

In this Appendix, we give the modifications that must be made to Dellago and Posch's [6] algorithm for calculating the Lyapunov spectrum of the hard-sphere fluid. We first present their results, and then our generalization.

One first calculates a trajectory $\mathbf{\Gamma}(t)$ of the system in phase space. The hard-sphere fluid has two types of motion. Between collisions, the system evolves continuously,

$$\dot{\mathbf{\Gamma}}=\boldsymbol{F}(\mathbf{\Gamma}), \tag{A1}$$

except at times $\{\tau_1,\tau_2,\ldots\}$, when the system moves instantaneously from one phase space point to another,

$$\mathbf{\Gamma}'=\boldsymbol{M}(\mathbf{\Gamma}). \tag{A2}$$

Along with $\mathbf{\Gamma}(t)$ one evolves a set of $4N$ infinitesimal Lyapunov vectors $\{\delta\mathbf{\Gamma}\}$ such that $\mathbf{\Gamma}(t)+\delta\mathbf{\Gamma}(t)$ is a trajectory in phase space distinct from, but infinitely close to $\mathbf{\Gamma}(t)$. The Lyapunov spectrum is calculated from the growth rate of these vectors. This set of $4N$ vectors must be periodically renormalized, as described in [25].

During the continuous part of the motion, the Lyapunov vectors $\delta\mathbf{\Gamma}$ evolve according to

$$\delta\dot{\mathbf{\Gamma}}=\frac{\partial\boldsymbol{F}}{\partial\mathbf{\Gamma}}\cdot\delta\mathbf{\Gamma}, \tag{A3}$$

and when the system jumps from one point to another, Dellago and Posch showed that the Lyapunov vectors transform according to

$$\delta\mathbf{\Gamma}'=\frac{\partial\boldsymbol{M}}{\partial\mathbf{\Gamma}}\cdot\delta\mathbf{\Gamma}+\left[\frac{\partial\boldsymbol{M}}{\partial\mathbf{\Gamma}}\cdot\boldsymbol{F}(\mathbf{\Gamma})-\boldsymbol{F}(\boldsymbol{M}(\mathbf{\Gamma}))\right]\delta\tau_c. \tag{A4}$$

The second term on the right hand side arises because the map $\boldsymbol{M}$ is not applied at the same time in the two trajectories. The particles are at slightly different positions so their collisions will occur at slightly different times. The quantity $\delta\tau_c$ is the difference in collision times.

It now becomes more convenient to use the notation

$$\mathbf{\Gamma}=\begin{pmatrix}\boldsymbol{r}\\ \boldsymbol{v}\end{pmatrix},\quad \delta\mathbf{\Gamma}=\begin{pmatrix}\delta\boldsymbol{r}\\ \delta\boldsymbol{v}\end{pmatrix},\quad \boldsymbol{r}=\begin{pmatrix}\vec{r}_1\\ \vec{r}_2\\ \vdots\\ \vec{r}_N\end{pmatrix}, \tag{A5}$$

where $\boldsymbol{r}$ and $\boldsymbol{v}$ are the position and velocity coordinates. (Recall that boldface vectors are phase space vectors while physical space vectors are indicated by an arrow.) Between collisions, we have free motion, so

$$\dot{\mathbf{\Gamma}}=\begin{pmatrix}\dot{\boldsymbol{r}}\\ \dot{\boldsymbol{v}}\end{pmatrix}=\begin{pmatrix}\boldsymbol{v}\\ \boldsymbol{0}\end{pmatrix}. \tag{A6}$$

The Lyapunov vectors obey

$$\dot{\delta\mathbf{\Gamma}}=\begin{pmatrix}\dot{\delta\boldsymbol{r}}\\ \dot{\delta\boldsymbol{v}}\end{pmatrix}=\begin{pmatrix}\delta\boldsymbol{v}\\ \boldsymbol{0}\end{pmatrix}. \tag{A7}$$

For hard spheres, the map applied at each collision is

$$\mathbf{\Gamma}'=\begin{pmatrix}\boldsymbol{r}'\\ \boldsymbol{v}'\end{pmatrix}=\begin{pmatrix}\boldsymbol{r}\\ \boldsymbol{v}+\vec{f}\boldsymbol{C}\end{pmatrix}. \tag{A8}$$

We have used slightly different notation than Dellago and Posch. The momentum transferred from one particle to another during the collision is $\vec{f}$:

$$\vec{f}=[(\vec{v}_B-\vec{v}_A)\cdot\hat{n}]\hat{n}, \tag{A9}$$

which is the same as Eq. (6) with $r=1$. As before, A and B label the two colliding particles, and $\hat{n}$ is a normal vector pointing from the center of B to the center of A. $\boldsymbol{C}$ is a vector that has 1 in the position of particle A, -1 in the position of particle B and 0 elsewhere. Thus $\vec{v}'=\vec{v}+\vec{f}\boldsymbol{C}$ means $\vec{v}_A'=\vec{v}_A+\vec{f}$, $\vec{v}_B'=\vec{v}_B-\vec{f}$, and $\vec{v}_i'=\vec{v}_i$ for $i\neq A,B$.

Equation (A4) becomes

$$\delta\boldsymbol{\Gamma}'=\begin{pmatrix}\delta\boldsymbol{r}'\\ \delta\boldsymbol{v}'\end{pmatrix}=\begin{pmatrix}\delta\boldsymbol{r}-\vec{f}\,\delta\tau_c\boldsymbol{C}\\ \delta\boldsymbol{v}+\vec{\delta f}\boldsymbol{C}\end{pmatrix}, \tag{A10}$$

where $\vec{\delta f}=(\partial\vec{f}/\partial\boldsymbol{\Gamma})\cdot\delta\boldsymbol{\Gamma}$. This transformation involves only the components of $\delta\boldsymbol{\Gamma}$ corresponding to the two colliding particles. This enables us to integrate Eqs. (A7) and (A10) rapidly. The algorithm proceeds as follows: for each particle, we store the time of its last collision (or τ_0, the time of the beginning of the simulation, if that particle has suffered no collisions). Suppose we are just about to treat collision n involving particles A and B. Before applying Eq. (A10), we must take into account the free motion leading up to collision n. Let j_A denote the index of A's last collision (where $j_A=0$ if this is A's first collision). For each Lyapunov vector $\delta\boldsymbol{\Gamma}$ we modify the components associated with particle A using

$$\delta\vec{r}_n=\delta\vec{r}_{j_A'}+\delta\vec{v}_{j_A'}(\tau_{j_A}-\tau_n). \tag{A11}$$

Here, $\delta\vec{r}_n$ is the phase space deviation just before collision n while $\delta\vec{r}_{j_A}'$ is the deviation just after collision j_A. Equation (A11) gives the change in these components of the Lyapunov vectors that has occurred during the free motion since collision j_A. After doing the same thing for particle B, we apply Eq. (A10). Finally, we set $j_A=j_B=n$ and go to collision $n+1$.

We now turn to the thermostatted ($r\neq1$) case. The algorithm must be modified, but it remains essentially the same. As we will see, instead of storing the time of each particle's last collision, we must store $8N+3$ quantities per particle. These additional quantities, however, play the same role as τ_{j_A} in Eq. (A11).

When the thermostat is applied, the map applied at collisions becomes

$$\begin{pmatrix}\boldsymbol{r}'\\ \boldsymbol{v}'\end{pmatrix}=\begin{pmatrix}\boldsymbol{r}\\ \boldsymbol{\epsilon}(\boldsymbol{v}+\vec{f}\boldsymbol{C})\end{pmatrix}, \tag{A12}$$

where $\boldsymbol{\epsilon}$, given in Eq. (8) is the factor needed to maintain constant energy. The momentum transfer is now given by Eq. (6), not Eq. (A9). Note that $\boldsymbol{\epsilon}$ multiplies all components of $\boldsymbol{v}$, not only those involved in the collision. Eq. (A4) becomes

$$\begin{pmatrix}\delta\boldsymbol{r}'\\ \delta\boldsymbol{v}'\end{pmatrix}=\begin{pmatrix}\delta\boldsymbol{r}+[(1-\boldsymbol{\epsilon})\boldsymbol{v}-\boldsymbol{\epsilon}\vec{f}\boldsymbol{C}]\delta\tau_c\\ \boldsymbol{\epsilon}\delta\boldsymbol{v}+\boldsymbol{\epsilon}\vec{\delta f}\boldsymbol{C}+\delta\boldsymbol{\epsilon}(\boldsymbol{v}+\vec{f}\boldsymbol{C})\end{pmatrix}, \tag{A13}$$

where $\delta\boldsymbol{\epsilon}=(\partial\boldsymbol{\epsilon}/\partial\boldsymbol{\Gamma})\cdot\delta\boldsymbol{\Gamma}$. Equation (A13) can be implemented directly, but the resulting program is very slow because all components of the displacement vectors must be modified at each collision. Furthermore, Eq. (A11) cannot be used because $\delta\boldsymbol{v}$ changes at each collision. We therefore seek an alternative that allows us to advance the coordinates associated with freely moving particles over many collisions at a time. We first search for a generalization of Eq. (A11) that gives the evolution of the noncolliding components of the Lyapunov vectors. Suppose that a particle undergoes free motion between τ_j and τ_n, i.e., it is not involved in any collision i with $j>i>n$. Let $\delta\vec{r}_j'$ and $\delta\vec{v}_j'$ be the phase space deviations just after collision j, and $\delta\vec{r}_n$ and $\delta\vec{v}_n$ are the deviations just before the collision n. The effect of repeated applications of Eq. (A13) for collisions i with $j>i>n$ give

$$\begin{pmatrix}\delta\vec{r}_n\\ \delta\vec{v}_n\end{pmatrix}=\begin{pmatrix}\delta\vec{r}_j'+B_{j+1}^n\delta\vec{v}_j'+(C_{j+1}^{n-1}+D_{j+1}^n)\vec{v}^*\\ E_{j+1}^{n-1}\delta\vec{v}_j'+A_{j+1}^{n-1}\vec{v}^*\end{pmatrix}. \tag{A14}$$

Here, $\vec{v}^*$ is the particle velocity with t as the time variable. It is constant between collisions. But the real content of Eq. (A14) lies in the following definitions:

$$E_m^n=\prod_{i=m}^{n}\boldsymbol{\epsilon}_i,$$

$$A_m^n=\sum_{i=m}^{n}E_{i+1}^n\delta\boldsymbol{\epsilon}_i/\gamma_i,$$

$$B_m^n=\sum_{i=m}^{n}E_m^{i-1}\gamma_{i-1}(\tau_i-\tau_{i-1}), \tag{A15}$$

$$C_m^n=\sum_{i=m}^{n}(1-\boldsymbol{\epsilon}_i)\delta\tau_{ci}/\gamma_i,$$

$$D_m^n=\sum_{i=m}^{n}A_m^{i-1}\gamma_{i-1}(\tau_i-\tau_{i-1}).$$

In these definitions, γ_i is the value of γ just before collision i, $\boldsymbol{\epsilon}_i$ is the value of $\boldsymbol{\epsilon}$ for collision i, $\delta\tau_{ci}$ is the value of $\delta\tau_c$ for collision i, etc. If $m>n$, we take $E_m^n=1$ and the sums equal to 0. We call these quantities ''propagators'' because the propagate the Lyapunov vectors forward in time through the collisions given by the super- and sub-script: the notation E_m^n is meant to suggest that this quantity propagates $\delta\boldsymbol{\Gamma}$ from collision m to collision n. Not all the superscripts in Eq. (A14) are the same because A, C, and E are incremented during the collision while B and D are incremented during the free motion leading up to the collision. Thus A, C, and E have a superscript of $n-1$ because collision n has not yet occurred. But B and D have a superscript of n because the free motion leading up to collision n has occurred. Note that A_m^n and D_m^n depend on $\delta\boldsymbol{\Gamma}$ (via $\delta\boldsymbol{\epsilon}$).

As one advances in time, it is easy to update these quantities. Suppose the collision n has just occurred. Then the free motion between collision n and $n+1$ can be taken into account using

$$B_m^{n+1} = B_m^n + E_m^n \gamma_n (\tau_{n+1} - \tau_n),$$
$$D_m^{n+1} = D_m^n + A_m^n \gamma_n (\tau_{n+1} - \tau_n). \tag{A16}$$

At collision $n+1$, we update the other three quantities,

$$A_m^{n+1} = \epsilon_{n+1} A_m^n + \delta\epsilon_{n+1},$$
$$C_m^{n+1} = C_m^n + (1-\epsilon_{n+1})\,\delta\tau_{cn+1}/\gamma_{n+1}, \tag{A17}$$
$$E_m^{n+1} = \epsilon_{n+1} E_m^n.$$

Now we are ready to give the new algorithm. In this algorithm, the propagators defined in Eq. (A15) play the same role as the time in Eq. (A11). One part of the algorithm consists in maintaining current values of all the propagators with subscript equal to 1. That is, after collision n, we have A_1^n, B_1^n, C_1^n, D_1^n, and E_1^n. At the beginning of the simulation, we have simply $A_1^0 = B_1^0 = C_1^0 = D_1^0 = 0$, and $E_1^0 = 1$. As the simulation advances, we first apply Eq. (A16) and then Eq. (A17) for each collision. This is sufficient to maintain the current values of the propagators. In addition, for each particle we store the value of the propagators just after its last collision. For example, if particle A's last collision is j_A, we store $A_1^{j_A}$, $B_1^{j_A}$, $C_1^{j_A}$, $D_1^{j_A}$, and $E_1^{j_A}$. Since different values of $A_1^{j_A}$ and $D_1^{j_A}$ must be stored for each $\delta\mathbf{\Gamma}$, this amounts to $8N+3$ numbers per particle. This requires a lot of memory ($8N^2$ numbers, but recall $\{\delta\mathbf{\Gamma}\}$ contains $16N^2$ numbers), but adds very little computation time. Each particle ''remembers'' the values of the propagators just after its last collision. Imagine that we want to treat collision n using Eq. (A14). We do not have necessary propagators. For example, we need $A_{j_A+1}^{n-1}$, but we have only $A_1^{j_A}$ and A_1^{n-1}. But the needed propagators can all be calculated from the available ones using

$$A_{j+1}^{n-1} = A_1^{n-1} - E_{j+1}^{n-1} A_1^j,$$
$$B_{j+1}^n = (B_1^n - B_1^j)/E_1^j,$$
$$C_{j+1}^{n-1} = C_1^{n-1} - C_1^j, \tag{A18}$$
$$D_{j+1}^n = D_1^n - D_1^j - A_1^j B_{j+1}^n,$$
$$E_{j+1}^{n-1} = E_1^{n-1}/E_1^j.$$

Once these relations are used, Eq. (A14) can be applied. The same procedure can be done for particle B. Then, the colliding components of the Lyapunov vectors can be updated using a partial application of Eq. (A13). The application is partial because only the colliding components must be changed. The changes to the uncolliding components called for by Eq. (A13) will be made later, during an application of Eq. (A14). At the end of the simulation and just before one of the periodic orthogonalizations, Eq. (A14) must be applied to all the components.

[1] G.P. Morriss, Phys. Rev. A **37**, 2118 (1988).
[2] D.J. Evans, E.G.D. Cohen, and G.P. Morriss, Phys. Rev. A **42**, 5990 (1990).
[3] S. Sarman, D.J. Evans, and G.P. Morriss, Phys. Rev. A **45**, 2233 (1992).
[4] W.G. Hoover and H.A. Posch, Phys. Rev. E **49**, 1913 (1994).
[5] E.G.D. Cohen, Physica A **213**, 293 (1995); E.G.D. Cohen, in *Dynamics: Models and Kinetic Methods for Non-equilibrium Many Body Systems*, Vol. 371 of *NATO Advanced Studies Institute Series E: Applied Sciences*, edited by J. Karkheck (Kluwer, Amsterdam, 2000).
[6] Ch. Dellago, H.A. Posch, and W.G. Hoover, Phys. Rev. E **53**, 1485 (1996); Ch. Dellago and H.A. Posch, Physica A **240**, 68 (1997).
[7] W.G. Hoover, *Time Reversibility, Computer Simulation and Chaos* (World Scientific, Singapore, 1999).
[8] H.A. Posch, R. Hirschl, and W.G. Hoover, in *Dynamics: Models and Kinetic Methods for Nonequilibrium Many Body Systems*, of Vol. 371, *NATO Advanced Studies Institute Series E: Applied Sciences*, edited by J. Karkheck (Kluwer, Amsterdam, 2000).
[9] W.G. Hoover, Phys. Rev. A **31**, 1695 (1985).
[10] J.R. Dorfman and P. Gaspard, Phys. Rev. E **51**, 28 (1995).
[11] P. Gaspard, Physica A **240**, 54 (1997).
[12] J.R. Dorfman and H. van Beijeren, Physica A **240**, 12 (1997).
[13] P.K. Haff, J. Fluid Mech. **134**, 401 (1983).
[14] I. Goldhirsch and G. Zanetti, Phys. Rev. Lett. **70**, 1619 (1993).
[15] S. McNamara and W.R. Young, Phys. Rev. E **53**, 5089 (1996).
[16] R. Brito and M.H. Ernst, Europhys. Lett. **43**, 497 (1998).
[17] R. Soto, M. Mareschal, and M.M. Mansour, Phys. Rev. E **62**, 3836 (2000).
[18] S. Chapman and T.G. Cowling, *The Mathematical Theory of Non-uniform Gases* (Cambridge University Press, Cambridge, 1939).
[19] Lj. Milanović and H.A. Posch, Chaos **8**, 455 (1998).
[20] H.A. Posch and R. Hirschl, in *Hard-Ball Systems*, edited by D. Szasz (Springer Verlag, Berlin, 2000).
[21] J.P. Eckman and O. Gat, J. Stat. Phys. **98**, 775 (2000).
[22] S. McNamara and M. Mareschal (unpublished).
[23] P. Frederikson, J. Kaplan, E. Yorke, and J. Yorke, J. Diff. Eqns. **49**, 185 (1983).
[24] G.P. Morriss, C.P. Dettmann, and L. Rondoni, Physica A **240**, 84 (1997).
[25] A. Wolf, J.B. Swift, H.L. Swinney, and J.A. Vastano, Physica D **16**, 285 (1985).